Single particle detection of protein molecules using dark-field microscopy to avoid signals from nonspecific adsorption

Author:
Markhali, BP; Sriram, M; Bennett, DT; Khiabani, PS; Hoque, S; Tilley, RD; Bakthavathsalam, P; Gooding, JJ

Publication details:
Biosensors and Bioelectronics
v. 169
Medium: Print-Electronic
0956-5663 (ISSN); 1873-4235 (ISSN)

Publication Date:
2020-12-01

Publisher DOI:
https://doi.org/10.1016/j.bios.2020.112612

Single particle detection of protein molecules using dark-field microscopy to avoid signals from nonspecific adsorption

Bijan P. Markhali[+], Manish Sriram[+], Danielle T. Bennett[+], Parisa S. Khiabani, Sharmin Hoque, Richard D. Tilley, Padmavathy Bakthavathsalam*, J. Justin Gooding*

School of Chemistry, Australian Centre for NanoMedicine and the ARC Centre of Excellence in Convergent Bio-Nano Science and Technology, The University of New South Wales, Sydney 2052, Australia.

[†] These authors contributed equally to this work.

* Corresponding author. E-mail address: justin.gooding@unsw.edu.au, p.bakthavathsalam@unsw.edu.au

Abstract

A massively parallel single particle sensing method based on core-satellite formation of Au nanoparticles was introduced for the detection of interleukin 6 (IL-6). This method exploits the fact that the localized plasmon resonance (LSPR) of the plasmonic nanoparticles will change as a result of core-satellite formation, resulting in a change in the observed color. In this method, the hue (color) value of thousands of 67 nm Au nanoparticles immobilized on a glass coverslip surface is analyzed by a Matlab code before and after the addition of reporter nanoparticles containing IL-6 as target protein. The average hue shift as the result of core-satellite formation is used as the basis to detect small amount of proteins. This method enjoys two major advantages. First it is able to analyze the hue values of thousands of nanoparticles in parallel in less than a minute. Secondly the method is able to circumvent the effect of non-specific adsorption, a major issue in the field of biosensing.

Keywords:

Single particle sensing

Ensemble detection

Protein

Antibody

Dark-field microscopy

Nonspecific adsorption

1. Introduction

Non-specific adsorption is a persistent challenge for most sensors. Non-specific adsorption occurs when an unwanted molecule attaches to the surface and produces a background noise that is indistinguishable from the signal from the specific binding of the analyte (Lichtenberg et al. 2019; Pan et al. 2017). It negatively effects the selectivity, specificity, and reproducibility of almost all types of interfacial biosensors (Ahluwalia et al. 1995; Lichtenberg et al. 2019; Ogi et al. 2009). It is a challenge that is exacerbated in proportion to the sensitivity of the sensor and it is particularly problematical for sensors where any change at the sensing interface causes a signal. The latter includes many refractive sensors, microbalance sensors and electrochemical impedance based sensors (Barfidokht and Gooding 2014). Traditional methods of reducing non-specific adsorption focus on using surface modification layers such as serum albumins (Jia et al. 2018; Minopoli et al. 2020; Riquelme et al. 2016; Sheikh et al. 2013; Wang et al. 2020), poly(ethylene glycol) (PEG) layers (Cerruti et al. 2008; Sharma et al. 2004; Su et al. 2019) or zwitterionic polymers (Baggerman et al. 2019; Cui et al. 2017; Wang et al. 2017). All these methods are incredibly successful at reducing the amount of non-specific adsorption up to or even greater than 99 %, although complete reduction has not yet been achieved. Other approaches explored include more dynamic methods such as applying oscillating shear forces which are stronger than the temporary adhesive forces of proteins weakly bound to the molecule (Lichtenberg et al. 2019). The needed shear forces can be generated by transducer-based electrochemical devices (Vaidyanathan et al. 2014; Wang et al. 2015), acoustic waves (Sankaranarayanan et al. 2008; Sankaranarayanan et al. 2010), or fluid based devices (Li et al. 2017). Both these strategies revolve around preventing non-specific binding occurring.

A different strategy to addressing non-specific adsorption is to design the sensor in a way that a different response is recorded by specific binding events compared with non-specific binding events, allowing the response from non-specific interactions to be identifiable. We first demonstrated such a strategy using porous silicon photonic crystals for monitoring enzyme activity where the specific enzyme activity causes a blue shift in the reflectance spectrum whilst ant non-specific adsorption causes a red shift (Kilian et al. 2009). More recently we have demonstrated this for plasmonic nanoparticles using a surface enhanced Raman scattering (SERS) approach where individual Raman dyes (Rhodamine 6G) were detected (Zheng et al. 2015). In that system the magnitude of the signal from the dye was far greater for the specific nanoparticles in the Raman hotspots when compared to the non-specific signal and thus they could be differentiated. We also showed that specific and non-specific signals for detecting proteins could be differentiated in a single molecule sandwich immunoassay using a nanopore blockade sensors (Chuah et al. 2019). What these latter two strategies demonstrate is that single nanoparticle sensors can have advantages in reducing the influence of nonspecific adsorption in carefully configured assays but neither of these approaches are compatible with massively parallel single nanoparticle sensing that is required to provide robust quantitative information similar to that achieved with ensemble sensors (Wu et al. 2019).

We previously showed that single molecule signals from thousands of plasmonic nanoparticles could be captured in dark-field images in a matter of seconds(Sriram et al. 2018a). This approach has the potential to be employed for massively parallel single particle detection. The purpose of this paper is to show the ability of massively parallel single particle detection to provide quantitative information, in this case for the cytokine interleukin 6 (IL-6) using a localized surface plasmon resonance (LSPR) sandwich assay, that is tolerant to nonspecific binding effects. The reason for choosing IL-6, a pro-inflammatory cytokine, was its involvement in many inflammatory diseases (Richard J. Simpson 1997) as well as its role in the different stages of many cancers (Ho et al. 2015; Tartour and Fridman 1998; Zhou Xing 1998). After confirming the potential of the dark-field sensor design to provide quantitative information, we focus on showing why the analytical signals from the dark-field sensor are insensitive to non-specific adsorption.

2. Materials and methods

2.1. Chemicals and materials

The following chemicals 1-ethyl-3-(3-dimethylaminopropyl)carbodiimide (EDC), *N*-hydroxysuccinimide (NHS), streptavidin, phosphate buffer saline (PBS), bovine serum albumin (BSA), (3-aminopropyl)triethoxysilane (APTES), sodium citrate tribasic dehydrate, gold (III) chloride trihydrate ($HAuCl_4.3H_2O$) were purchased from Sigma-Aldrich (Sydney, Australia). Active human IL-6 full length, monoclonal anti-IL-6 antibody, polyclonal anti-IL-6 antibody (Biotin), 3,3′,5,5′-tetramethylbenzidine (TMB), goat anti-rabbit IgG H&L (HRP), were purchased from Abcam (Australia), 10 nm and 20 nm gold nanoparticles were purchased form nanoComposix (USA), small glass coverslips (22 x 22 mm, 0.16-0.17 mm thickness) were supplied by Thermo Scientific (Australia), monocarboxy(1-mercaptoundec-11-yl)hexa(ethylene glycol) (HS-OEG) was purchased from ProChimia Surfaces (Poland), boric acid, ethanol 96%, ethanol, hydrogen peroxide, sodium tetraborate, and boric acid were supplied by Chem-Supply (Australia) and sulfuric acid was purchased from Merck (Australia). The water used was Milli-Q grade (18 MΩ cm) (Millipore Australia) unless otherwise stated.

2.2. Gold nanoparticle synthesis

Different sizes of Au nanoparticles were synthesized by following the method of Bastus et al (Bastús et al. 2011). Briefly, a solution of 2.2 mM sodium citrate in 150 mL Milli-Q water was heated in a 250 mL three necked round bottom flask for 15 min. Vigorous stirring was performed during heating. A condenser was used to avoid evaporation. When the solution started boiling 1 mL of $HAuCl_4$ with a concentration of 25 mM was added to the system. After 10 min, a pink solution forms indicating gold seed formation. This solution was then cooled to 90 °C. To grow the seeds to the desired size, of 1 mL aliquots of 25 mM $HAuCl_4$ was added in 30 min intervals twice. At this point a 55 mL aliquot of Au nanoparticle solution was removed from the solution using a syringe. This aliquot contained the smallest Au nanoparticles. Larger particles were then grown using the previous particles as seeds. To achieve this, 53 mL of Milli-Q water and 2 mL of 60 mM sodium citrate are added to the seed solution. Following this, three consecutive additions of 1 mL of 25 mM $HAuCl_4$ was added every 30 min before another aliquot of nanoparticles was collected. The growth and collection

procedure was repeated six more times to achieve a batch of Au nanoparticles of different sizes. The nanoparticles are citrate capped and depending on the conditions used, a batch can have an average size distribution ranging from 27 nm to 100 nm. Specifications of these synthesized nanoparticles are listed in Table SI1.

3. Surface preparation and immobilization of 67 nm Au nanoparticles.

To immobilize gold nanoparticles on a glass coverslip the procedure (depicted in Fig.SI1 in supplementary materials) was employed. First the surface was silanized using APTES. To do so, the surfaces were first immersed in piranha solution (3:1 mixture of H_2SO_4:H_2O_2) for 45 min followed by extensive rinsing with Milli-Q water and ethanol. Then the coverslips were immersed in a solution containing 90% v/v ethanol, 5% v/v water, and 5% v/v APATES and left for 1.5 h. Then the coverslips were rinsed with ethanol and Milli-Q water and stored in ethanol at 4 °C for at most 1 week prior use. Au nanoparticles with average diameter of 67 nm were diluted (1:10) and put on surface for 15 min. Then the surfaces were washed and dried. The coverslips with immobilized Au nanoparticles were immediately used in the project.

3.1. Functionalization of 67 nm Au nanoparticles

To attach monoclonal anti-IL-6 antibody to 67 nm Au nanoparticles (hereafter we call the core nanoparticles), first a monolayer of HS-OEG was self-assembled onto the core nanoparticles surface by adding a solution of 2 mM HS-OEG in Milli-Q water to the coverslips and leaving it overnight. The surface was subsequently washed thoroughly with Milli-Q water. The monoclonal anti-IL-6 antibodies were attached to the core nanoparticles by using EDC/NHS to couple amine moieties of the antibodies to carboxylic acid end of OEG. Fig. SI1 (supplementary materials) shows the process in detail. Briefly a solution of EDC (104 mM) and NHS (208 mM) in water was added to the surfaces and left for 1 h. Then the surface was washed with Milli-Q water and anti-IL-6 antibodies (10 μg/mL) were dropped on the surface and left for 2 h. Finally the surface was washed thoroughly and dried with a nitrogen blow.

3.2. Functionalization of 10 nm Au nanoparticles

To attach the biotinylated polyclonal anti-IL-6 antibodies to 10 nm Au nanoparticles (hereafter referred to as reporter nanoparticles) as depicted in Fig.SI2, first streptavidin was attached to reporter nanoparticles physically by pH control. The pH was adjusted to 8.11 through a buffer exchange with borate buffer. A 200 µL Au nanoparticle solution (5 nM) was centrifuged at 4000 rpm for 30 min, in an Eppendorf tube, and the supernatant was removed. Then the resulted pellet was resuspended in borate buffer (pH 8.11). The procedure was repeated 2 more times. Streptavidin was then added to gold nanoparticles and incubated for 1 h with gentle shaking. Then the nanoparticles were washed three times in MilliQ and centrifuged before resuspending them in a solution of biotinylated polyclonal anti-IL-6 antibodies (50 ng/mL) and incubated for 1 h at room temperature under laminar flow. Finally, to remove excess antibodies, the reporters were centrifuged in PBS containing 1 w/v BSA three times and resuspended in 1 mL of the same buffer. Fig. SI2 (supplementary information) shows a schematic representation of functionalization of reporter nanoparticles.

3.3. Dark-field microscopy and image analysis

The dark-field microscopy was performed using an Olympus BX51 microscope. The excitation source was a 100 W halogen lamp and was focused through a dark-field condenser (NA > 0.8). A 40X objective lens was used for taking the picture using a commercial CMOS camera (Canon 100D, 22.3 mm x 14.9 mm sensor size, 4.3 µm x 4.3 µm pixel size). The images were saved and processed as Canon RAW (.CR2) 14 bit color files.

The image analysis was performed using an in-house written MATLAB algorithm, the detail of which was explained in our previous work (Sriram et al. 2018b). The calculated hue values for each spot was used for detection of IL-6.

3.4 Electron microscopy imaging

To make the glass coverslip conductive, before SEM imaging the coverslips were mounted on conductive stubs and then were coated with a 5 nm layer of Pt using a Leica EM ACE600 sputter coater. SEM imaging was performed on a field emission scanning electron microscope, Nova NanoSEM model. Transmission electron microscopy (TEM) measurements were carried out using the Phillips CM200 and images were captured with a SIS CCD camera attached to the microscope.

3.5 Electromagnetic simulation

Comsol Multiphysics™ was used to model two dimensional plasmonic structures. Here the light wave electromagnetic waves module was used. A core 70 nm Au and 1 and 2 satellite with size of 10, 20, 30, and 40 nm were modelled. For the 2 satellite structure both symmetric and asymmetric configurations were modelled. The gap between core and satellites were 10 nm. The wavelength was set to scan from 400 nm to 700 nm with a resolution of 1 nm. A scattering boundary was used to avoid reflection off the boundary of simulation. The simulation was performed assuming the environment around the nanoparticles was air. The boundary had a radius of 700 nm. Relative permeability of the protein was assigned to be 0.49. The refractive index of the antibody was varied from 1.40-1.42 with the corresponding thickness outlined in the work of Pollitt et. al (Pollitt et al. 2015).

4. Results and discussions

The proposed biosensor utilizes the fact that a dark-field optical microscope can acquire images of Au nanoparticles in which the color of the scattered light changes when a core-satellite is formed. Scheme 1 shows the workflow of the process. Here 67 nm Au nanoparticles were chosen as core nanoparticles because the light scattered from these gold plasmonic nanoparticles is relatively sharp and is located in the visible spectrum, causing them to appear green. As depicted in Scheme 1. A), a coverslip with immobilized 67 nm Au nanoparticles, which are modified with anti-IL-6 monoclonal antibodies, are the biorecognition interface of the dark-field microscopy sensor. The 67 nm Au nanoparticles appear as green dots, thousands of which may be captured per dark-field image (Fig.SI3 in supplementary information). The coverslip was then exposed to the sample solution comprised of IL-6 and 10 nm reporter nanoparticles modified with polyclonal anti-IL-6 antibodies (Fig. S13B). Capturing of the IL-6 by the reporter nanoparticles allows the formation of a core-satellite assembly with 67 nm Au core nanoparticles on the surface. The formation of the core-satellite assembly is shown in the transmission electron microscopy images (TEM) shown in Fig.SI4 in the supplementary information. Note if the IL-6 is absent, some reporter nanoparticles are observed on the coverslip but they are not located adjacent to the core nanoparticles. The scattering spectrum, measured through the hue of the core-satellite assemblies in the dark-field images were then expected to be discernable from single 67 Au nanoparticle as a result of the shift in their color from green to orange/red (Sriram et al. 2018a) (Scheme 1.).

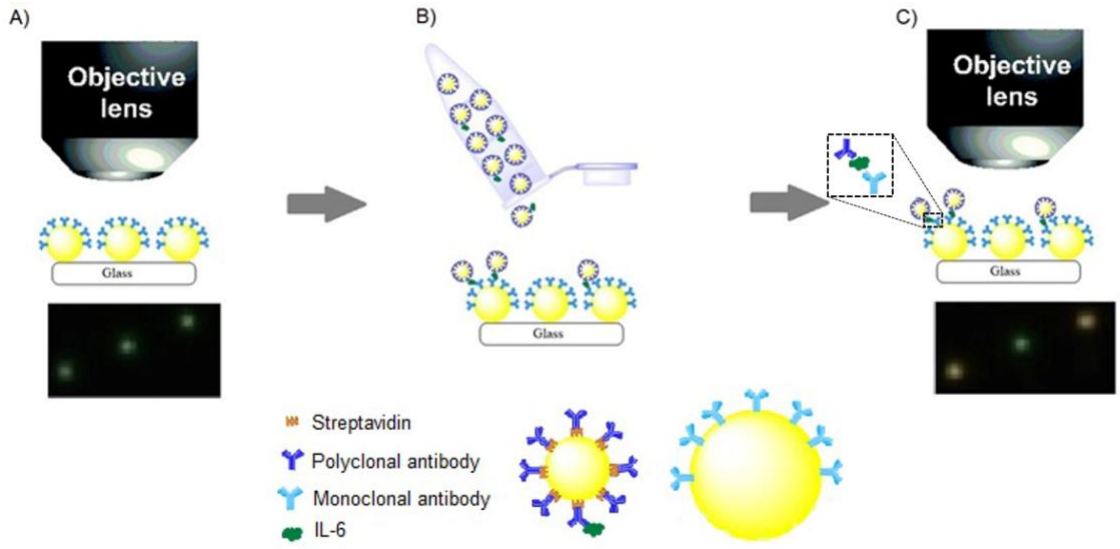

Scheme 1: Schematic workflow of the experiment. A) Cover slip surface with immobilized 67 nm Au nanoparticles modified with monoclonal antibody under dark-field microscopy are seen as green dots. B) Addition of reporter nanoparticles containing the antigen to the surface. Reporter nanoparticles containing antigen will form core-satellite assemblies with the 67 nm Au nanoparticles immobilized on the surface. C) The coverslip surface under dark-field microscopy after addition of reporter nanoparticles and formation of core-satellite assemblies. The formation of assemblies will be evident by a shift in the hue of the nanoparticles to an orange/reddish color.

Fig. 1. shows representative results from the workflow depicted in Scheme 1. Fig. 1A and Fig. 1B are dark-field images of a coverslip before and after addition of the solution of reporter nanoparticles when there is 40 ng/mL of IL-6 present in solution, respectively. It should be noted that only a cropped part of the actual dark-field images is displayed for clarity. Fig. 1A and Fig. 1B show a significant shift in the color of the core nanoparticles when reporters with IL-6 bind to form the core-satellite. Histograms of the color shift from the average particle hue for the total dark field images of Fig. 1A and Fig. 1B are shown in Fig. 1C (Sriram et al. 2018a). This shift in hue from average hue value of the nanoparticles before and after the addition of reporter nanoparticles could be used to quantify the performance of the biosensor. In this case, the average hue before addition of reporter nanoparticles was 0.388 and after addition of reporter nanoparticles the hue changed to 0.205, a -0.183 shift in hue. Fig. 1D and Fig. 1E show the dark-field images of the control, a coverslip before and after addition of the solution of reporter nanoparticles in the absence of IL-6. Similarly, Fig. 1F shows the corresponding color analysis histograms for images in Fig. 1D and Fig. 1E. In the absence of IL-6, from an original hue of 0.354 a shift in hue of less than 0.007 was observed which confirms that core-satellite assemblies are being formed only with the antibody molecule as a linker.

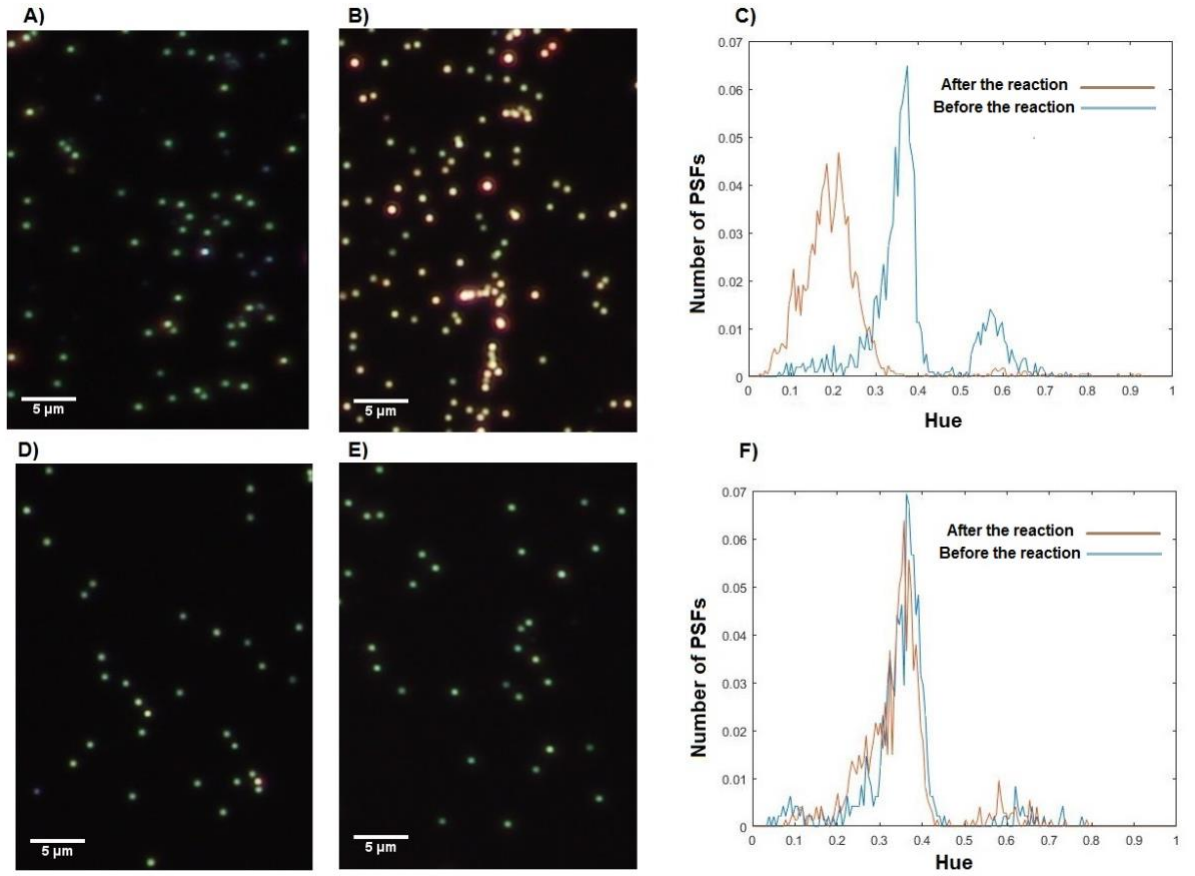

Fig. 1. A) and B) are respectively the dark-field images of the cover slip surface before and after addition of the solution of reporter nanoparticles with 40 ng/mL of IL-6 as antigen. C) The corresponding result of color analysis for A) and B). The color shift is visible with the naked eye and is quantified using the color analysis code. D) and E) are dark-field images of the coverslip surface before and after the addition of the solution of reporter nanoparticles with 0 ng/mL IL-6 respectively. F) Histogram of color analysis performed on images D) and E) using the color analysis code where there is no IL-6 added.

SEM images of the surfaces were taken to further validate that the color shift of -0.184 in hue occurs due to formation of core-satellite assemblies. Fig. SI5 shows representative SEM images of surfaces corresponding to samples with and without IL-6. These figures show that 10 nm satellites only bind around the core whilst IL-6 is present. It is worth noting that despite non-specific adsorption of the antibody modified satellites on the surface, they did not have any effect on the background signal of the sensor since nanoparticles smaller than 40 nm are undetectable through traditional dark-dark field microscopy (Zijlstra and Orrit 2011). This observation confirms that the hue shift observed under dark-field microscopy is indeed due to formation of core-satellite assemblies when reporter nanoparticles have captured the target analyte IL-6.

The magnitude of the shift in the average hue value is dependent on the concentration of IL-6 which shows the method can form the basis of a quantitative sensor. Fig. 2. shows the calibration curve for the average change in hue as a function of concentration. The lowest detected concentration of 0.01 ng/mL still gave a signal well above the baseline. The theoretical detection limit of three times the standard deviation of the blank was 7 pg/mL. To put this detection limit in context, the provider of the antibodies (Abcam) have stated that for the antibody-antigen sandwich used in this experiment, the two main conventional methods used for the detection of IL-6 (Huang et al. 2013; Singh et al. 2017; Taton et al. 2000), ELISA and Western blot, have a detection limit in the order of 0.500 ng/mL. That is, this dark-field approach is showing an impressive 50 fold decrease in detection limit over the conventional methods using the same antibodies.

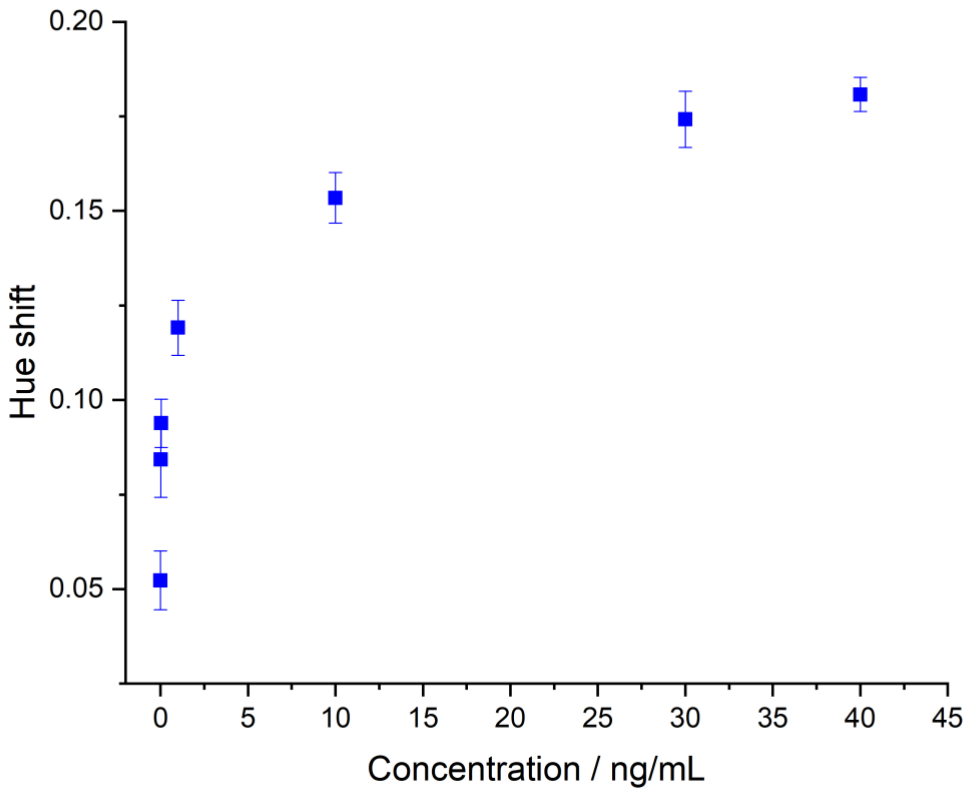

Fig. 2. Calibration curve of sensor. For each concentration 3 repeats were performed. Each dot is the average hue shift of the surface. To obtain the error bars, the standard deviation from average hue in 3 repeats, was calculated.

The findings so far have thus demonstrated that the darkfield sensor can provide quantitative sensing information when used as an ensemble sensor based on the average responses across the surface. However, to understand the virtue of the signal coming from many individual surfaced bound core nanoparticles we need to investigate the signal changes at the single nanoparticles level over many nanoparticles. By mapping the locations of individual nanoparticles within images before and after the addition of reporters the color shift of thousands of individual nanoparticles can be determined in a matter of seconds. To map a specific region on the sensing surface and allow individual nanoparticle shifts to be calculated, a simple spot mapping approach (Fig. SI6 in supplementary information) was employed. Fig.SI3. depicts the results of such a mapping exercise. Each image contains thousands of spots, each of which is a nanostructure. The code finds the location of each particle using their relative intensity and can calculate the hue of the pixels around each individual spot in a matter of seconds. After addition of the antigen and reporter nanoparticles, those same locations are revisited and the hues sampled again to observe their shift. This allows for a massively parallel investigation of single nanoparticle to be conducted within seconds.

As previously mentioned non-specific adsorption is a persistent challenge in the field of biosensing which negatively affects the performance of biosensors. In the current design, the following scenarios are the possible ways for non-specific adsorption to occur:

1. Adsorption of reporter nanoparticles on the free spaces of the surface.
2. Adsorption of proteins, molecules and impurities in the free spaces of the surface.
3. Nonspecific adsorption of reporter nanoparticles on the surface of core nanoparticles.
4. Adsorption of unwanted molecules on the surface of core nanoparticles.

Addressing points 1 and 2 above, Fig. 3A and Fig. 3B show the dark-field and SEM images of a surface after the addition of reporter nanoparticles, respectively. In Fig. 3B many nonspecifically absorbed reporter nanoparticles can be seen, but they do not appear in the dark-field image. The absence of a nonspecific signal with the reporter nanoparticles is because they are below the minimum size of around 40 nm where the intensity of the scattered light is too weak to be visible during dark-field microscopy and thus is not visible in the resulting image (Boyer et al. 2002). Thus, although the presence of reporter nanoparticles binding to the sensing surface, as shown in Fig. 3D), they do not contribute to the signal, and hence preventing their nonspecific adsorption is unnecessary. This is in contrast to a

traditional plasmonic surface where the binding of gold nanoparticles to a gold surface would cause a plasmonic shift, and highlights the virtues of using many single nanoparticle measurements to obtain the analytical signal over a single plasmonic surface. It is only when the reporter nanoparticles bind to the core nanoparticles that a color change is observed in the scattered light in the dark field image. For large clusters, since we record dark-field images of the same area before and after addition of reporter nanoparticles, the image analysis code can identify and exclude any spot on the dark-field image which is related to these clusters. Similarly, large impurities which are spotted on the dark-field image could be excluded from analysis by the code while most of nonspecifically adsorbed proteins on the surface are too small to form a darkfield spot.

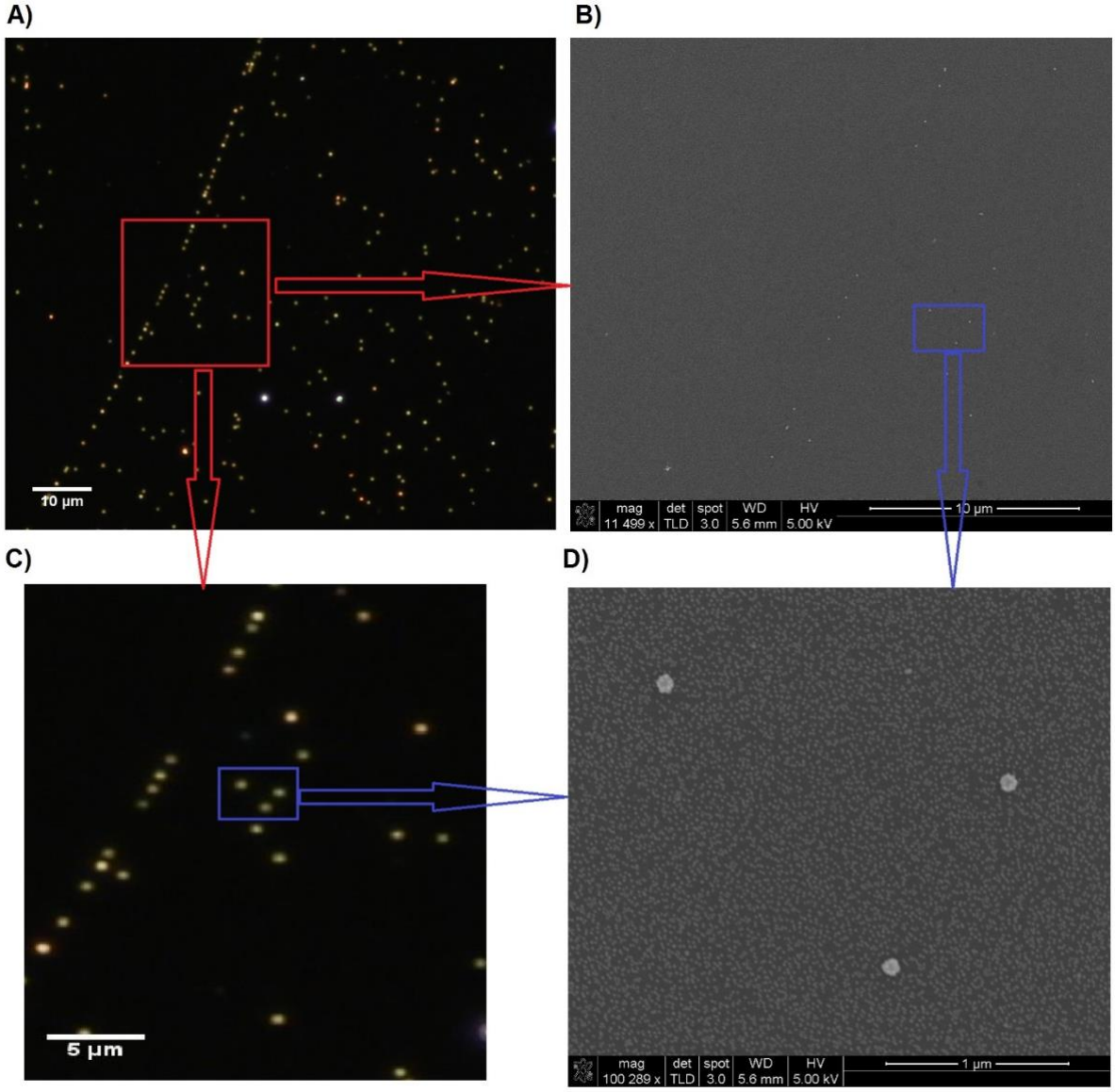

Fig. 3. Dark-field and scanning electron microscopy images of the same location on a surface. A) dark-field image of the surface after addition of 10 nm reporter nanoparticles containing 40 ng/mL IL-6. B)

and C) are SEM and zoomed in dark-field image of the red area shown in part A). D) is the zoomed in SEM image of the blue areas depicted in parts B) and C). Part D) provides evidence that while the surface is covered by non-specifically adsorbed 10 nm reporter nanoparticles they do not contribute to the shift in hue of the 67 nm core nanoparticles and only the assembly of satellites onto the nanoparticle cores causes the shift.

Regarding the third case, where reporter nanoparticles are non-specifically attached to the core nanoparticles, there are two ways we envisage this could happen. The first is when reporter nanoparticles that have not captured any proteins attach to the core. It was shown in Fig. 1D-F and Fig. SI5B that this does not occur. The other possibility is when a protein other than the target analyte binds to the reporter nanoparticles and then the reporter nanoparticle binds to the core nanoparticle. That is the wrong protein forms the immuno-sandwich; this is something considered exceedingly unlikely as sandwich assays are one way of improving selectivity considerably as the selectivity of two antibodies are employed (Wu et al.). To explore whether this type of non-specific adsorption could occur we compared the ensemble hue shifts (Fig. 4A) and individual nanoparticle shifts (Fig. 4B) after the additional of 10 ng/mL IL-6) and compared this to when 40 ng/mL IL-11 was added (Fig. 4C) and D) as the 'wrong' antibody. With the addition of Il-11 a slight color shift (hue: 0.029) toward red values was observed, which can be related to the nonspecific adsorption. In contrast, when the correct protein analyte, 10 ng/mL IL-6, was present then a 0.12 hue shift was recorded. It can be seen from the single particle analysis approach (Sriram et al. 2018a) that the 0.12 hue shift (Fig 4B) was due to many single particles shifting whilst with the IL-11 (Fig. 4D) very few of the individual particles showed a hue change. Note that the absence of shifts due to incorrect binding of the reporter nanoparticles to the core particles not causing a shift is hue is despite that fact that reporter nanoparticles do nonspecifically adsorb to the underlying surface. However, this nonspecific adsorption of reporter nanoparticles does not cause a spectral shift as they are too small. Of course this exemplifies the benefits of recording analytical data from many single nanoparticles as such nonspecific adsorption would definitely cause nonspecific signals if the substrate was a gold film.

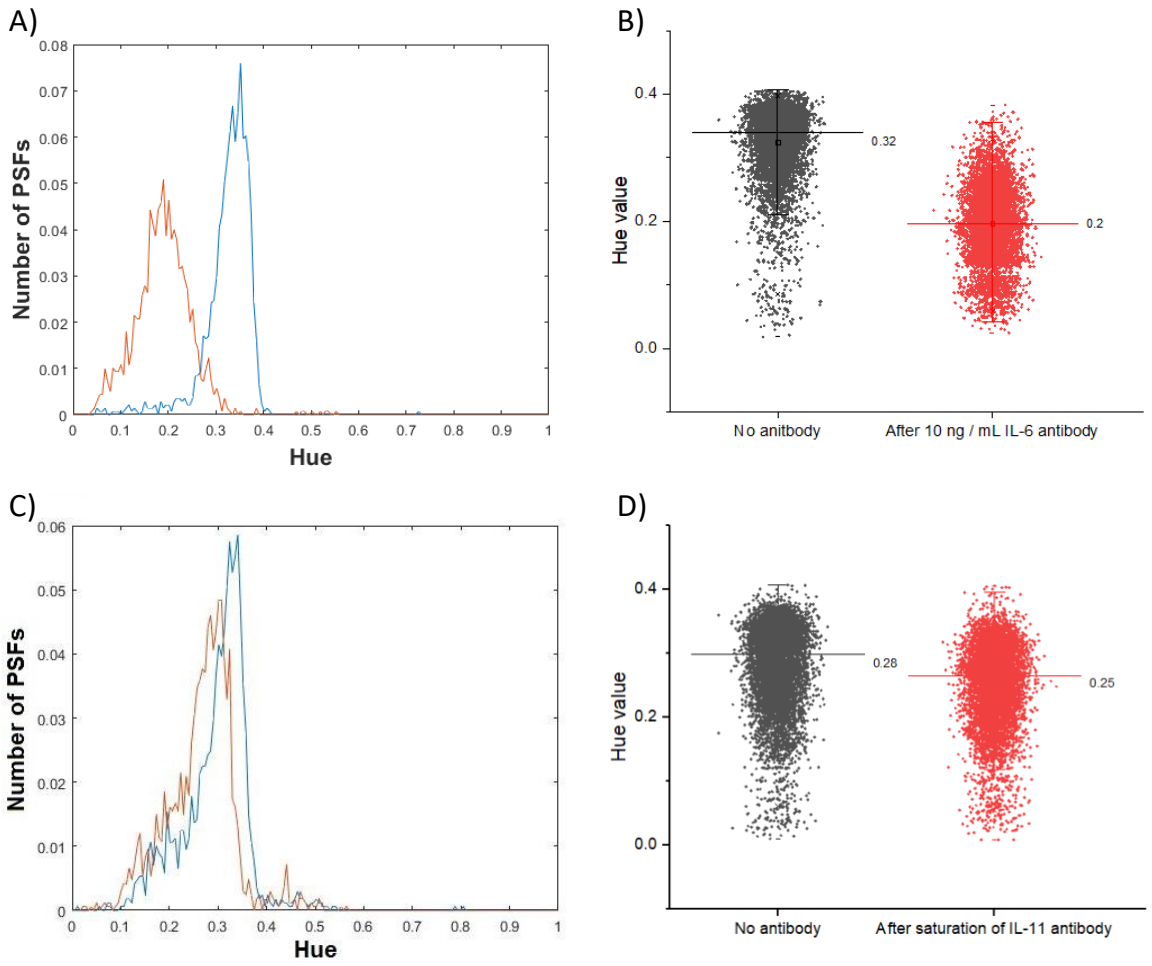

Fig. 4. A comparison between ensemble and single molecule sensing for the same sample. A) is the ensemble measurement of a surface treated with 10 ng/mL of IL-6 and B) is the individual particle analysis of that same surface. Similarly C) shows the ensemble measurement of a surface before and after addition of the 'wrong' antibody IL-11 and D) shows the individual hue of each particle of the same image, C) This reveals that the 'wrong' antibody shifts very little in comparison with the positive surface.

With regards to the fourth case where protein molecules non-specifically adsorb onto the core nanoparticles, a COMSOL simulation was conducted. The goal here was to calculate the possible color shift of the system when in an extreme case all the surface of the core is covered with a layer of non-specifically attached proteins. The simulated spectra are shown in Fig. 5. From the figure it can be observed that even if the core nanoparticles are completely covered by a layer of non-specifically adsorbed proteins, the peak shift is negligible (<1 nm) and so does not interfere with the color analysis. This is as distinct from when a 10 nm reporter nanoparticles where, a shift of ~ 12 nm is calculated (Fig. 5B) for a single reporter binding to the core nanoparticle. Note to obtain the spectrum with the 10 nm reporter particles the gap between the cores and reporter nanoparticles was set to 10 nm as

determined using dynamic light scattering measurements (Fig. SI7 in supplementary information) and TEM (Fig. SI4 in supplementary information). The 12 nm shift is slightly is excellent agreement with the ~12 nm average shift in the experimental system shown in Fig. 4B) suggesting that for at the concentration of 10 ng/mL Il-6 there is typically one reporter particle attached to the core nanoparticles that exhibit shifts in hue.

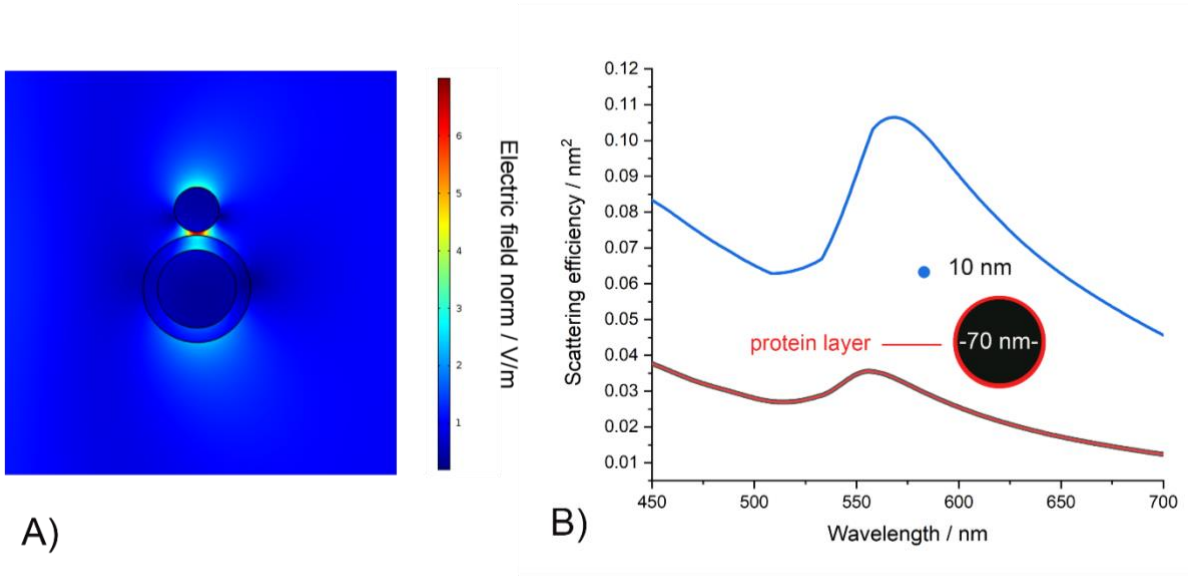

Fig. 5. shows the calculated scattering cross-section of core-satellite assemblies. A) shows the Comsol™ setup of the core, protein layer, and satellite arrangement, with the electric field norm superimposed. B) shows the scattering efficiency for simulations with 70 nm diameter cores showing that a bare core and core with a 14 nm antibody layer shows no discernible shifting. Also shown is the spectral shift when a 10 nm reporter nanoparticle binds to the core as in A) to show the shift in scattering efficiency.

Conclusion

Based on our previous proposed method (Sriram et al. 2018b) firstly a sandwich assay LSPR colorimetric biosensor was introduced. The method results in a fast analysis of color values of thousands of nanoparticles simultaneously when single protein binding events bring together antibody core and satellite nanoparticles into close proximity with a concomitant shift in the plasmonic spectra. The viability of the sensor was confirmed for detecting the cytokine IL-6 as an ensemble sensor giving an average plasmonic spectral shift across the whole surface. TEM and dark-field microscopy imaging however shows that the system allows the measurement of single nanoparticle events.

The advantage of moving to measurements from individual nanoparticles is the method becomes very tolerant to nonspecific adsorption. Four scenarios of nonspecific adsorption was investigated. These were 1) nonspecific adsorption of reporter nanoparticles between surface bound core nanoparticles, 2) non-specific adsorption of proteins and impurities between surface bound core nanoparticles, 3) nonspecific adsorption of reporter nanoparticles on the surface of core nanoparticles or 4) non-specific adsorption of proteins onto the surface of core nanoparticles. The experimental results show that in all cases none of these cases occurred, or they gave insignificant shifts in the spectra, compared with the correct formation of the core-satellite immunosandwich in the presence of the target analyte. These conclusions were supported by a computational investigation that showed that 10 nm reporter nanoparticles gave a sufficiently large color shift after core-satellite formation, to overcome any nonspecific adsorption effects from proteins in solution. As such the results suggest it is possible using this size of reporter nanoparticle to construct assays based on massively parallel measurement of single particle binding events, have the potential to lead to massively parallel single molecule counting in complex media. This could be the subject of further studies. It is important to note that the tolerance of the massively parallel single nanoparticle assays is not just relevant for potential single molecule counting experiments. The results presented herein also show that for ensemble measurements across the entire surface, sensors are more robust and tolerant to nonspecific adsorption than if the substrate was a continuous gold film. Thus, how design of the single nanoparticle assays, where the measurement is only responsive to the formation the core nanoparticle-reporter nanoparticle pairs when the correct antigen is present, provides one solution to an enduring challenges in plasmonic sensors of nonspecific adsorption causing erroneous signals.

Acknowledgements:

We acknowledge the financial support for this research from the Australian Research Council (ARC) through the ARC Centre of Excellence in Convergent Bio-Nano Science and Technology (CE140100036) and the ARC Laureate Fellowship (FL150100060). This work was also supported through access to the Australian National Fabrication Facility (ANFF) Design House software at the NSW node of ANFF.

References:

Ahluwalia, A., Giusto, G., De Rossi, D., 1995. Non-specific adsorption on antibody surfaces for immunosensing. Materials Science and Engineering: C 3(3-4), 267-271.
Baggerman, J., Smulders, M.M., Zuilhof, H., 2019. Romantic Surfaces: A Systematic Overview of Stable, Biospecific, and Antifouling Zwitterionic Surfaces. Langmuir 35(5), 1072-1084.
Barfidokht, A., Gooding, J.J., 2014. Approaches Toward Allowing Electroanalytical Devices to be Used in Biological Fluids. Electroanalysis 26(6), 1182-1196.
Bastús, N.G., Comenge, J., Puntes, V., 2011. Kinetically controlled seeded growth synthesis of citrate-stabilized gold nanoparticles of up to 200 nm: size focusing versus Ostwald ripening. Langmuir 27(17), 11098-11105.
Boyer, D., Tamarat, P., Maali, A., Lounis, B., Orrit, M., 2002. Photothermal imaging of nanometer-sized metal particles among scatterers. Science 297(5584), 1160-1163.
Cerruti, M., Fissolo, S., Carraro, C., Ricciardi, C., Majumdar, A., Maboudian, R., 2008. Poly(ethylene glycol) Monolayer Formation and Stability on Gold and Silicon Nitride Substrates. Langmuir 24(19), 10646-10653.
Chuah, K., Wu, Y., Vivekchand, S.R.C., Gaus, K., Reece, P.J., Micolich, A.P., Gooding, J.J., 2019. Nanopore blockade sensors for ultrasensitive detection of proteins in complex biological samples. Nature Communications 10.
Cui, M., Wang, Y., Jiao, M., Jayachandran, S., Wu, Y., Fan, X., Luo, X., 2017. Mixed self-assembled aptamer and newly designed zwitterionic peptide as antifouling biosensing interface for electrochemical detection of alpha-fetoprotein. ACS sensors 2(4), 490-494.
Ho, L.-J., Luo, S.-F., Lai, J.-H., 2015. Biological effects of interleukin-6: Clinical applications in autoimmune diseases and cancers. Biochemical pharmacology 97(1), 16-26.
Huang, J., Harvey, J., Fam, W.D., Nimmo, M.A., Tok, I.A., 2013. Novel biosensor for Interleukin-6 detection. Procedia Engineering 60, 195-200.
Jia, S., Bian, C., Sun, J., Tong, J., Xia, S., 2018. A wavelength-modulated localized surface plasmon resonance (LSPR) optical fiber sensor for sensitive detection of mercury (II) ion by gold nanoparticles-DNA conjugates. Biosensors and Bioelectronics 114, 15-21.
Kilian, K.A., Lai, L.M.H., Magenau, A., Cartland, S., Bocking, T., Di Girolamo, N., Gal, M., Gaus, K., Gooding, J.J., 2009. Smart Tissue Culture: in Situ Monitoring of the Activity of Protease Enzymes Secreted from Live Cells Using Nanostructured Photonic Crystals. Nano Letters 9(5), 2021-2025.

Li, D., Wang, C., Sun, G., Senapati, S., Chang, H.-C., 2017. A shear-enhanced CNT-assembly nanosensor platform for ultra-sensitive and selective protein detection. Biosensors and Bioelectronics 97, 143-149.
Lichtenberg, J.Y., Ling, Y., Kim, S., 2019. Non-Specific Adsorption Reduction Methods in Biosensing. Sensors 19(11), 2488.
Minopoli, A., Sakač, N., Lenyk, B., Campanile, R., Mayer, D., Offenhäusser, A., Velotta, R., Della Ventura, B., 2020. LSPR-based colorimetric immunosensor for rapid and sensitive 17β-estradiol detection in tap water. Sensors and Actuators B: Chemical, 127699.
Ogi, H., Fukunishi, Y., Nagai, H., Okamoto, K., Hirao, M., Nishiyama, M., 2009. Nonspecific-adsorption behavior of polyethylenglycol and bovine serum albumin studied by 55-MHz wireless–electrodeless quartz crystal microbalance. Biosensors and Bioelectronics 24(10), 3148-3152.
Pan, S., Zhang, H., Liu, W., Wang, Y., Pang, W., Duan, X., 2017. Biofouling removal and protein detection using a hypersonic resonator. ACS sensors 2(8), 1175-1183.
Pollitt, M.J., Buckton, G., Piper, R., Brocchini, S., 2015. Measuring antibody coatings on gold nanoparticles by optical spectroscopy. Rsc Advances 5(31), 24521-24527.
Richard J. Simpson, A.H., David K. Smith, Jacqueline M. Matthews, Larry D. Ward, 1997. Interleukin-6: Structure-function relationships. Protein Science 6, 929-955.
Riquelme, M.V., Zhao, H., Srinivasaraghavan, V., Pruden, A., Vikesland, P., Agah, M., 2016. Optimizing blocking of nonspecific bacterial attachment to impedimetric biosensors. Sensing and bio-sensing research 8, 47-54.
Sankaranarayanan, S.K., Cular, S., Bhethanabotla, V.R., Joseph, B., 2008. Flow induced by acoustic streaming on surface-acoustic-wave devices and its application in biofouling removal: A computational study and comparisons to experiment. Physical Review E 77(6), 066308.
Sankaranarayanan, S.K., Singh, R., Bhethanabotla, V.R., 2010. Acoustic streaming induced elimination of nonspecifically bound proteins from a surface acoustic wave biosensor: Mechanism prediction using fluid-structure interaction models. Journal of Applied Physics 108(10), 104507.
Sharma, S., Johnson, R.W., Desai, T.A., 2004. XPS and AFM analysis of antifouling PEG interfaces for microfabricated silicon biosensors. Biosensors and Bioelectronics 20(2), 227-239.
Sheikh, S., Blaszykowski, C., Thompson, M., 2013. Sacrificial BSA to block non-specific adsorption on organosilane adlayers in ultra-high frequency acoustic wave sensing. Surface and interface analysis 45(11-12), 1781-1784.
Singh, M., Truong, J., Reeves, W., Hahm, J.-i., 2017. Emerging cytokine biosensors with optical detection modalities and nanomaterial-enabled signal enhancement. Sensors 17(2), 428.
Sriram, M., Markhali, B.P., Nicovich, P.R., Bennett, D.T., Reece, P.J., Brynn Hibbert, D., Tilley, R.D., Gaus, K., Vivekchand, S.R.C., Gooding, J.J., 2018a. A rapid readout for many single plasmonic nanoparticles using dark-field microscopy and digital color analysis. Biosensors and Bioelectronics 117, 530-536.
Sriram, M., Markhali, B.P., Nicovich, P.R., Bennett, D.T., Reece, P.J., Hibbert, D.B., Tilley, R.D., Gaus, K., Vivekchand, S., Gooding, J.J., 2018b. A rapid readout for many single plasmonic nanoparticles using dark-field microscopy and digital color analysis. Biosensors and Bioelectronics 117, 530-536.

Su, H., Li, S., Kerman, K., 2019. Novel thiolated-PEG linker molecule for biosensor development on gold surfaces. Biosensors and Bioelectronics 141, 111477.
Tartour, E., Fridman, W., 1998. Cytokines and cancer. International reviews of immunology 16(5-6), 683-704.
Taton, T.A., Mirkin, C.A., Letsinger, R.L., 2000. Scanometric DNA array detection with nanoparticle probes. Science 289(5485), 1757-1760.
Vaidyanathan, R., Naghibosadat, M., Rauf, S., Korbie, D., Carrascosa, L.G., Shiddiky, M.J.A., Trau, M., 2014. Detecting Exosomes Specifically: A Multiplexed Device Based on Alternating Current Electrohydrodynamic Induced Nanoshearing. Analytical Chemistry 86(22), 11125-11132.
Wang, G., Han, R., Su, X., Li, Y., Xu, G., Luo, X., 2017. Zwitterionic peptide anchored to conducting polymer PEDOT for the development of antifouling and ultrasensitive electrochemical DNA sensor. Biosensors and Bioelectronics 92, 396-401.
Wang, Q., Wang, X.-Z., Song, H., Zhao, W.-M., Jing, J.-Y., 2020. A dual channel self-compensation optical fiber biosensor based on coupling of surface plasmon polariton. Optics & Laser Technology 124, 106002.
Wang, Y., Vaidyanathan, R., Shiddiky, M.J.A., Trau, M., 2015. Enabling Rapid and Specific Surface-Enhanced Raman Scattering Immunoassay Using Nanoscaled Surface Shear Forces. ACS Nano 9(6), 6354-6362.
Wu, Y., Bennett, D., Tilley, R.D., Gooding, J.J., 2019. How Nanoparticles Transform Single Molecule Measurements into Quantitative Sensors. Advanced Materials, 1904339.
Wu, Y.F., Bennett, D., Tilley, R.D., Gooding, J.J., How Nanoparticles Transform Single Molecule Measurements into Quantitative Sensors. Adv. Mater., 8.
Zheng, Y., Soeriyadi, A.H., Rosa, L., Ng, S.H., Bach, U., Justin Gooding, J., 2015. Reversible gating of smart plasmonic molecular traps using thermoresponsive polymers for single-molecule detection. Nature Communications 6(1), 8797.
Zhou Xing, J.G., Gerard Cox, Heinz Baumann, Manel Jordana, Xue-Feng Lei, Michelle K. Achong, 1998. IL-6 Is an Antiinflammatory Cytokine Required for Controlling Local or Systemic Acute Inflammatory Responses. J.Clin.Invest. 101, 311-320.
Zijlstra, P., Orrit, M., 2011. Single metal nanoparticles: optical detection, spectroscopy and applications. Rep. Prog. Phys. 74(10), 55.